ELSEVIER

Journal of Nuclear Materials 248 (1997) 64–71

journal of nuclear materials

Profiling with tritium imaging

I. Youle, A.A. Haasz *

University of Toronto Institute for Aerospace Studies, 4925 Dufferin St., North York, Ont., Canada M3H 5T6

Abstract

The tritium imaging technique focuses secondary electrons produced by β-particles emerging from a surface as a means of mapping the distribution of tritium in that surface. The short range of β-particles makes this technique sensitive to the depth of the tritium. The effect of tritium depth on the intensity of tritium images was investigated by several means. Specimens of different materials were implanted with 20 keV tritium ions, and imaged. The depth of the implanted tritium was decreased by sputtering the surface, while monitoring variations in image intensity. In graphite the image intensity increased as the depth of tritium was reduced, then decreased as sputtering began to remove the tritium itself. In aluminum, rapid tritium diffusion and large changes in surface conditioning had a strong effect on image intensity. It was, however, possible to measure intensity variations in one of the graphite specimens as increasingly thicker layers of aluminum were evaporated onto the surface. In this case surface conditioning effects were minimized by making measurements immediately after deposition. The results of both sets of experiments are interpreted using a theoretical curve which was based on the transport of primary beta particles to the surface. By introducing a light source, the imaging apparatus could be made to function as a photoelectron microscope. In this mode, changes in surface conditioning of deposited aluminum surfaces were observed. © 1997 Elsevier Science B.V.

1. Introduction

In the pursuit of magnetically confined nuclear fusion, the interaction of fuels, and particularly tritium, with material surfaces is of considerable interest with respect to safety, economics, component durability and an understanding of the fuel cycle. Means for detecting and measuring tritium in materials are necessary for research in these areas. The work described here was undertaken in order to quantify what has hitherto been merely a qualitative technique for examining tritium in materials.

The steady radioactive decay of tritium present on or just below a material surface will result in the emission of electrons from that surface. By means of an appropriate system of electrostatic lenses, these electrons may be focused to produce an image of the tritium in the surface. This process is referred to as tritium imaging [1].

In practice, focusing the β-particles that emerge from such a surface is difficult, due to their broad, 0–18 keV energy spectrum. However, as they leave the surface, they eject secondary electrons with less than 10 eV energy. The secondary yield of tritium β's is of order one. Because of their uniformly low energy, secondaries are easily accelerated and focused to form the desired tritium image by means of simple electrostatic lenses at reasonable (0–5 kV) potentials.

Tritium imaging has been used as a qualitative tool to monitor tritium in graphite and numerous metals [1–4]. Quantitative interpretation of images is difficult because of the many processes which occur in the production of an image. Transport of β-particles to the surface and secondary production at the surface are two important influences which, if other conditions can be held constant, ought to have a combined effect that is strictly a function of the depth of the tritium below the surface. This work describes measurements of this function in graphite and aluminum. It will be of use in the determination of depth profiles through alternate steps of sputtering and imaging.

* Corresponding author. Tel.: +1-416 667 7717; fax: +1-416 667 7743.

0022-3115/97/$17.00
PII S0022-3115(97)00150-5

2. Apparatus

2.1. Vacuum system

The experiments described here were carried out in a bakeable, stainless steel, ultrahigh vacuum chamber, evacuated with a turbomolecular pump. The pumping speed of the system was set by a 38 mm all-metal valve connecting the chamber and the pump; the ultimate pressure in the chamber was 1×10^{-5} Pa. This was adequate for imaging, but did allow an oxide layer to form on freshly deposited or sputtered aluminum surfaces in a relatively short time.

2.2. Electron optics

The essential parts of the apparatus are shown in Fig. 1. The specimen to be imaged is electrically grounded and forms the cathode of a three-element immersion lens [5]. The grid and anode consist of two aligned apertures, at potentials of $\sim +100$ V and $\sim +4000$ V respectively. Most of the imaging described here was done with a cathode-grid distance of 3 mm, resulting in a magnification of $\sim 8\times$, and a field of view of ~ 3 mm diameter. Lateral spatial resolution is of the order of 20 μm.

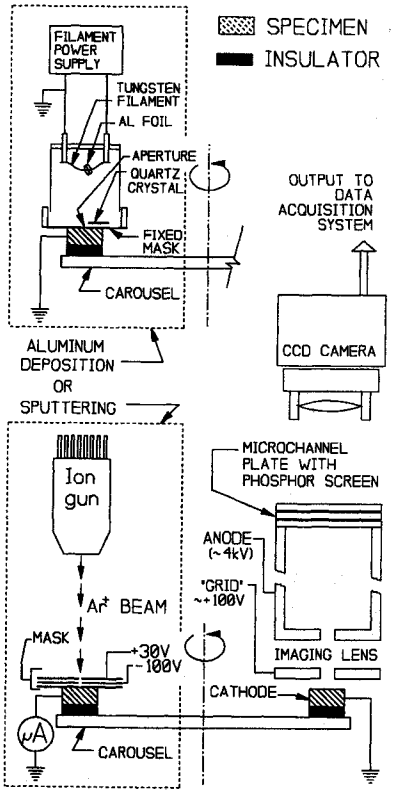

Fig. 1. Experimental apparatus showing the tritium imager, carousel, and the sputtering and Al deposition configurations. The vacuum envelope is not shown.

A chevron microchannel plate electron multiplier assembly [6] is placed at the image plane of the lens. Incoming single electrons are multiplied and accelerated onto a phosphor screen, where they produce a brief flash. The screen, which is inside the vacuum chamber, is monitored through a viewing port by a CCD television camera which transmits its images to machine-vision hardware incorporated in a personal computer. The rate of imaging electron production is such that the phosphor screen typically shows a few tens or hundreds of flashes at a time. It is necessary for the image processing section of the computer to add a few thousand or tens of thousands of individual images together, to produce a detailed picture of the tritiated region.

Specimens are mounted on a carousel, so that they can be adjusted to the best position under the imager, or moved to a second station in the vacuum chamber where they could be either sputtered or coated with aluminum. A telescope with a graticule eyepiece allows the operator to view alignment marks on the carousel, and adjust specimen position with a precision of about 0.05 mm. The carousel can also be raised and lowered a total distance of about 20 mm with a precision of 0.1 mm or better, in order to vary cathode-grid distance during imaging, or to position the specimen properly for sputtering or aluminum deposition.

2.3. Data acquisition and processing

Each time the CCD camera rasters once, the resulting picture of the phosphor screen, referred to as a frame, is sent to the image processing board, and digitally filtered. In the filtering process, all pixels with a value greater than a certain threshold are given a value '1', while those less than the threshold are given a value '0'. The threshold is set so that when a secondary electron is emitted from the specimen and focused on the microchannel plate, the resulting spot on the phosphor screen is bright enough that its image in the CCD frame exceeds the threshold. This will be referred to as an event. There will typically be several events per frame. The filtered frame is added (accumulated) to a frame buffer. The image is the result of accumulating a sufficient number of frames in the frame buffer. We define the *image intensity*, I, as the number of events per pixel per frame of the accumulated image, averaged over the region of interest.

The overall sensitivity of the microchannel plate is quite dependent on the voltages applied, cathode-grid distance, etc. To compensate for this, the image intensity in a region of interest (where sputtering, deposition, etc. may be occurring) is divided by the average intensity of a specific nearby unaltered 'reference' region, to yield the *relative intensity* of the region in question. Relative intensities tend to be more stable and reproducible than the image intensities defined above.

The sensitivity of the microchannel plate varies slightly over its surface. A completely unfocused image, or an image of the so-called 'dark current', will show corresponding variations in intensity. Dividing the pixel intensity of a focused image of a specimen by that of an unfocused image yields a *corrected image*, in which variations in micro-channel plate sensitivity occurring in both images cancel one another.

2.4. Sputtering

A 5 keV Ar^+ ion beam (~ 10 μA) can be directed at the tritiated specimen through a three-electrode sputtering mask. The first electrode touches the specimen, and its 1 mm diameter aperture defines the region to be sputtered. The second electrode is biased at ~ -100 V, and suppresses secondary electrons from the specimen and the other two electrodes. The purpose of the third electrode is to shield the second electrode from the ion beam, intercepting nearly 95% of it in the process. When focused, the ion beam had a full-width-at-half-height of 2 mm and was rastered 2.5 mm in each direction to ensure a uniform average ion flux over the entire 1 mm diameter aperture of the sputtering mask. A Faraday cup was used to determine the actual Ar^+ flux incident on the specimen.

At 5 keV, it is assumed that Ar^+ has a sputtering yield of 1.0 C/Ar on graphite, and 1.8 Al/Ar on aluminum [7].

2.5. Aluminum deposition

In some experiments, the ion gun was replaced with an aluminum deposition apparatus. Deposition was carried out by evaporation, using resistively heated tungsten filaments wrapped in aluminum foil. The apparatus used for these experiments had three separate filaments, spaced closely together over a fixed mask with a 1 mm diameter aperture. A thin film thickness monitor consisting of a 5.07 MHz quartz crystal was placed adjacent to the aperture. It was possible, with some care, to deposit a few nm of aluminum in a controlled fashion or up to 300 nm at one time. In general, the aluminum on the filaments was depleted fairly rapidly, requiring venting of the vacuum and replacement of the filaments after every 3–6 depositions.

2.6. Specimen preparation

The graphite specimens used in these experiments were $9 \times 12 \times 0.8$ mm^3 pieces of Union Carbide HPG99 'as-deposited' Pyrolytic Graphite mounted in aluminum specimen holders and implanted through a mask with a mass-selected beam of 26.7 keV HT. The T:H mass ratio resulted in an energy of 20 keV for the incident tritons. The intended density of implanted tritium was 10^{20} T/m^2, however lack of secondary electron suppression resulted in a measured beam current that was spuriously high. One specimen was burned, and the combustion products were analyzed using scintillation techniques to yield a measurement of areal tritium density of $\sim 2.5 \times 10^{19}$ T/m^2. Specimens used in the present experiments are believed to have similar areal tritium densities. The estimated depth profile of the implanted tritium, (Fig. 2), was calculated using the TRVMC (TRIM vectorized for multicomponent targets) computer code [8]. It has been shown that tritium implanted in graphite is immobile below 600 K [9], so the calculated profile can be assumed for all experiments with graphite.

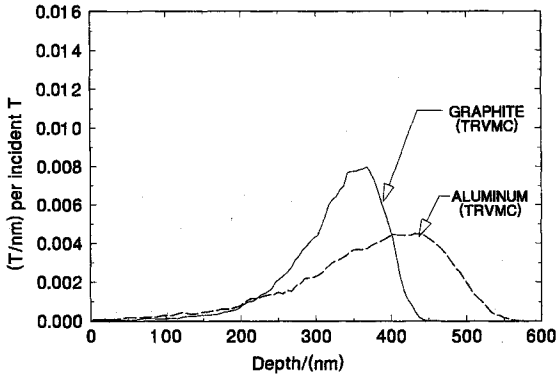

Fig. 2. Calculated depth distribution of implanted 20 keV tritium ions in graphite and aluminum, obtained from TRVMC Code [8].

The aluminum specimen was polished and implanted with 26.7 keV HT to a nominal density of 10^{20} T/m^2, although for similar reasons the exact amount of tritium in the specimen is unknown.

Because the amount of tritium in our specimens is not well established, we will avoid drawing conclusions concerning absolute image intensities. However, the fact that implantation was carried out at a well-defined voltage allows us to measure relative changes of image intensity as a function of the depth of tritium below the surface.

3. Experimental results

3.1. Depth profiling of graphite specimens

After the implanted graphite specimens were placed in the imaging system, they were alternately imaged and sputtered by means of the 5 keV Ar^+ ion beam. This experiment was repeated four times, at four different locations on the specimen. For each sputtered location, the relative intensities of corrected images were plotted, and smooth curves were drawn through the resulting scatter plots; each set of points and its associated smooth curve were then normalized so that the smooth curve assumes a value of unity at a depth of sputtering of 75 nm, see Fig. 3. This depth was chosen because it appears to be in the midst of a reasonably linear region of each of the curves, but does not lie near the calculated depth of implantation of the tritium, see Fig. 2.

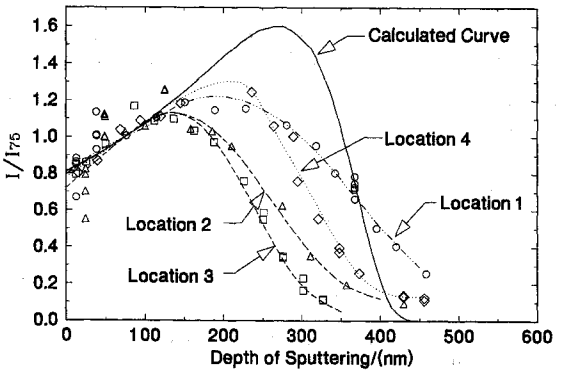

Fig. 3. Variations of relative image intensity as a function of sputtered depth in a tritium-implanted pyrolytic graphite specimen. The calculated curve is discussed in Section 4.

Each set of experimental points appears fairly self-consistent, being well approximated by the appropriate smooth curve, the data at location #2 being substantially the least regular. Although the curves for the separate sets of data have some variation, they have certain features in common. All have an initial linear region from the beginning of the sputtering to a 'turnover' region at a depth of 120–150 nm. The slopes in the initial linear region varied only slightly from 0.0027 nm^{-1} to 0.0036 nm^{-1}. The 'turnover' region is about 80 nm wide, except for the data from location #1, where it appears almost twice as wide. All curves then have a linear region of decreasing image intensity with similar slopes. As the image intensity approaches zero, there is a little tail, as the second derivative becomes positive. The four runs vary mainly in the locations of their maxima, and the maximum depths associated with each curve, which range from 350 nm to ~ 500 nm.

The differences in the experimentally observed curves are thought to be the result of inaccuracies in determining the total depth of sputtering. This is despite the fact that the voltages, including secondary electron suppression, were carefully maintained throughout the sputtering process. The possibility exists of some sort of redeposition of sputtered material, which might affect the apparent rate at which sputtering occurs, although it should be noted that there are no obvious trends in any properties of the curves as we go from the first run at location #1 to the last run at location #4.

The calculated curve shown in Fig. 3 will be discussed in Section 4, below.

3.2. Depth profiling of aluminum specimens

Sputtering was carried out at two different locations on the aluminum specimen. The different runs were not entirely consistent, but both indicate processes that are very different from the case of graphite; see Fig. 4. At the first location, the relative image intensity nearly doubled after sputtering only about 3 nm. By 10 nm, the relative image intensity had peaked. Further sputtering decreased the intensity at a fairly rapid rate, with the intensity finally approaching the background value by about 200 nm.

At the second location, the intensity of the sputtered region increased only slightly, and not very uniformly, as the first few nanometers were sputtered. Then, throughout most of the sputtered region, the relative image intensity fell monotonically. However, more intense patches, typically less than 0.1 mm in extent, would appear, and then, with further sputtering, abruptly shrink or fade to match the rest of the sputtered region, as if a thin tritiated layer was being removed in a slightly irregular fashion. By the time ~ 60 nm had been removed, there were no bright patches left, and the image intensity was fairly uniform, and falling over the entire sputtered region.

Two conclusions can be drawn from these results. First, because the image intensity was observed to increase substantially in the first run after only about 3 nm of sputtering, it is evident that the intensity is strongly influenced by the surface conditions of the specimen. It is well known that aluminum surfaces readily acquire thin oxide (alumina, Al_2O_3) coatings, and sputtering would rapidly remove such a layer and change the nature of the surface. The secondary electrons produced at the surface have extremely short ranges, so secondary production is governed entirely by the composition of the surface itself. If the image intensity had dropped suddenly after light sputtering, it would have been possible that all the tritium had segregated to the surface and been sputtered, but the observed, sudden increase in intensity can only be accounted for by a change in surface conditions.

Secondly, TRVMC Code calculations [8] indicate that the implanted tritium will stop at a slightly greater depth in aluminum (mean = 368 nm) than in graphite (331 nm); see Fig. 2. It is evident that the implanted tritium has migrated towards the surface of the specimen because of the very substantial drop in image intensity that occurs between 10 and 100 nm of sputtering. The diffusion constant, D_H, of

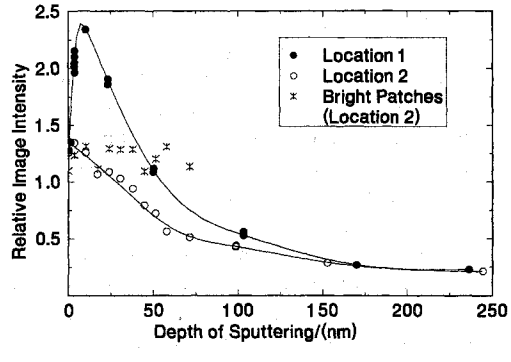

Fig. 4. Relative image intensity as a function of sputtered depth in a tritium-implanted aluminum specimen.

hydrogen in aluminum at room temperature is $\sim 10^{-13}$ m^2/s [10]. The specimen in question had been implanted a couple of years before the experiments described here, and so would have a characteristic diffusion length of

$$l = \sqrt{D_H t} = \sqrt{10^{-13}\ \frac{m^2}{s} \times 10^8\ s} \simeq 3\ mm. \quad (1)$$

That is to say, the implanted tritium could easily have diffused throughout the specimen, which was approximately 1 mm thick. Indeed, times on the order of one second would be sufficient to allow the tritium to diffuse a micrometer, which is of the order of the expected maximum depth of imaging. It is obvious that tritium has been trapped at the surface of the specimen, although it is unlikely that it is trapped in the surface oxide, in which hydrogen is known to have a low solubility [10]. It is more likely held in traps near the oxide–metal interface. This is consistent with observations made by others that for implantation densities of about 10^{20} H/m^2, the implanted hydrogen is trapped within a few tens of nanometers of the surface, even though the original depth of implantation may be somewhat greater [11]. It has also been observed [12] that hydrogen implanted at these fluences does not form observable bubbles.

No convincing explanation has been devised to account for the differences between the two curves of Fig. 4. It is thought that sputtering at the first location may have changed the surface conditions at the nearby second location, perhaps as a result of sputter products 'creeping' along between the mask and the specimen.

3.3. Aluminum deposition experiments

It is clear that tritium mobility and surface conditioning strongly influence image intensity in aluminum specimens. In order to eliminate these effects, relative tritium image intensity was measured for an implanted graphite specimen to which coatings of aluminum of varying thickness had been applied; see Fig. 5. This is not entirely satisfactory, as the tritium in the graphite is at some depth from the surface already, and the resulting overburden consists of a layer of graphite covered by a layer of aluminum. Additionally, tritium β's which may be initially directed into the bulk may be backscattered differently in graphite and aluminum. These factors could affect the variation of image brightness with tritium depth in aluminum.

Only measurements taken immediately after deposition (within ~ 3 min) were considered, because the image intensities of deposited aluminum surfaces were observed to rise with time, up to 40%, in the hours following the last deposition. Under the chamber pressure of 4×10^{-5} Pa, it is believed that a surface oxide layer gradually forms which increases the secondary electron yield and hence the image intensity.

The results of these measurements are shown in Fig. 5.

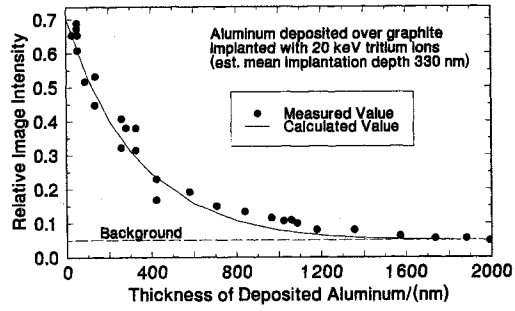

Fig. 5. Relative image intensity of tritium-implanted graphite, covered with an evaporated aluminum film, as a function of film thickness. The relative intensity at the same location of the bare graphite before any deposition was 1.04. All measurements were taken within 3 min of aluminum deposition, to insure a clean, oxide-free surface.

The calculated curve shown was derived from theoretical considerations of primary β transport to the surface, described in Section 4, below, with an added small constant background component, equal to the minimum measured relative intensity values (0.05).

3.4. Effects of surface conditions on tritium images

An important process in tritium imaging, which we have assumed to be reasonably constant in most of these experiments, is the production of secondary electrons at the surface. Because the range of secondaries is very short, on the order of nanometers, conditions exactly at the surface are the determining factor in secondary yield.

In graphite, sputtering a small amount of material from the original surface has a small effect on image brightness, indicating that the secondary electron yield of a sputtered surface is not much different from the original surface.

The intensity of tritium images of aluminum varied as the surface became oxidized. It appears that a slightly oxidized aluminum surface has a higher secondary electron yield than a new, clean one, in keeping with published results indicating that, as in the case of most metals, the photoelectric work function of alumina is lower than that of the unoxidized metal [13]. On the other hand, the image intensity of a two-year-old aluminum specimen stored at atmospheric pressure was increased by sputtering; see Section 3.2.

Variations in surface properties, especially with respect to electron emission can be demonstrated by running the imager as a photoemission electron microscope. It was observed that if the light used to illuminate the interior of the vacuum chamber during adjustment of the specimen was left on during imaging of an unoxidized aluminum surface, produced either by deposition of a new aluminum film, or by sputtering the surface of an old aluminum specimen, a very intense image of the surface was pro-

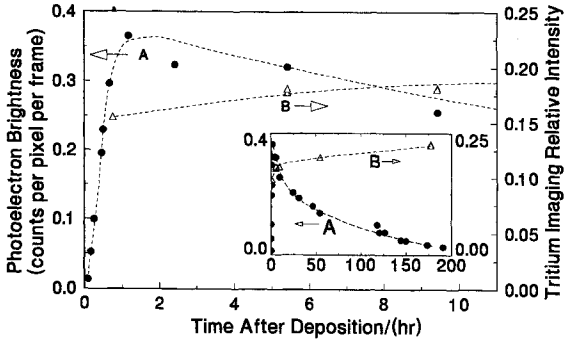

Fig. 6. Evolution of photoelectric image intensity (measured with light source on), and relative tritium image intensity (measured with light source off) on a deposited aluminum surface as a function of time. Chamber pressure was $\sim 4\times10^{-5}$ Pa.

duced. The light used here was a 60 W incandescent bulb located outside a viewing port, about 200 mm from the specimen being imaged, and shining very obliquely on the specimen during imaging. The photoemission image is independent of the presence of tritium in the material.

After depositing a fresh layer of aluminum of ~ 50 nm thickness, the specimen was viewed in 'photoelectric mode', and the image intensity of the deposited region noted at various times. It was found that the image intensity of the deposited region changed enormously, increasing by a factor of nearly thirty between five and seventy minutes after deposition, then falling slowly, taking over a week to approach about 1/15th of its maximum value. (See Fig. 6, curve A.) Had the experiment proceeded longer, it seems certain that the photoelectric image would have faded completely. The background pressure in the vacuum system for these experiments was 4×10^{-5} Pa. Exposure of the specimen to air was found to decrease its photoelectric image intensity to zero, or at least well below the tritium image intensity. The rate at which photoemission brightness changed did not appear to depend on whether the light source was left on or off between imaging, or on whether the chamber ionization gauge was operating or not. The physics of these observations is still unresolved, but the measurements are indicative of large changes in the nature of at least some property of the surface.

Interspersed with these measurements, some tritium images (with the light source turned off) were also taken. These showed much less variation with time than the photoelectric imaging. Relative intensity increased monotonically, by about 20% in the first few hours, and another 20–30% over the next week; see Fig. 6, curve B. This increase in intensity will be attributable to changing surface conditions if the diffusion of tritium from the sample up into the deposited layer is either unimpeded, and thus, according to Eq. (1), very rapid, or else completely suppressed by the oxide layer existing on the surface of the original sample. On the other hand, if the oxide layer impedes but does not entirely prevent tritium diffusion, some of the observed change in intensity may be due to the upward motion of tritium towards the surface.

4. Discussion and analysis

To relate tritium image intensity to tritium depth profile, we will assume the existence of a function $D(x)$, the *depth dependence of intensity*, which expresses the contribution of the tritium at some depth, x, per areal density of tritium at that depth, to the total image intensity.

We express the tritium distribution as the product of the total areal density, A, and a normalized depth distribution $C(x)$, such that $\int C(x)\,dx = 1$. Then, between x and $x + dx$, the areal density of tritium is $A\,C(x)\,dx$, and its contribution to the image intensity will be

$$dI = D(x)\,A\,C(x)\,dx \tag{2}$$

or, in integral form,

$$I = \int D(x)\,A\,C(x)\,dx, \tag{3}$$

where I is the experimentally measurable image intensity.

In order to estimate $D(x)$, an existing Monte Carlo program, MCSET [14], originally designed to model beta flux from the surface of uniform tritide materials, was modified to calculate the probability that a tritium beta produced at a given depth will emerge from the surface. The results for graphite are shown in Fig. 7. Details of these calculations will be given in a later publication.

Eq. (3) was numerically integrated, using the calculated implantation distribution for graphite from Fig. 2 as $C(x)$ and the β-emergence probability function in Fig. 7 as $D(x)$. Using this function as $D(x)$ admittedly fails to take into account the variations in secondary yield of the emerging β particles, and the probability of detection of

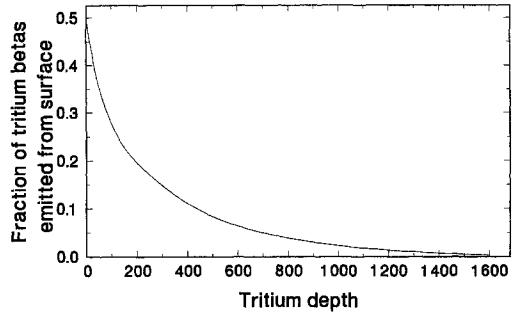

Fig. 7. The calculated probability, as a function of depth, that a β particle produced by a tritium decay will emerge from the surface of a flat dense (2260 kg/m^3) graphite specimen.

those secondaries, and is therefore, at best, an approximation, although under some circumstances, it may be shown that these two neglected factors may be relatively constant. The results of the integral are shown as the calculated curve in Fig. 3. The peak of this calculated curve, at a depth of about 250 nm corresponds roughly to the depth where the tritium density is rising sharply, (see Fig. 2). This is to be expected, since the decline in image intensity is due to the removal of tritium, and therefore will occur at the point where the tritium density becomes significant. The measured intensity profiles have peaks at generally much smaller depths. There are two possible causes of this. First, the tritium may actually be deposited at a shallower depth. This is fairly unlikely, as TRVMC has been shown to be in good agreement with experimental measurements of hydrogen implantation in graphite [15], and is generally considered to be more accurate than the widely-used TRIM95 [16], which, it must be noted, does predict shallower tritium deposition. The other possibility is that our sputtering yield is larger than expected, which would mean that the observed maximum intensity is at greater depths than the measurements would indicate. Also, because the observed profiles were normalized with respect to their values at 75 nm sputtering depth, increasing the estimate of sputtering yield would increase the height of the observed peaks slightly.

The calculated curve for aluminum deposited on graphite in Fig. 5 was also produced by assuming $D(x)$ could be approximated by the curve shown in Fig. 7, and using the fact that the range of β particles in materials is proportional to $A/\rho Z$, where A is atomic weight, ρ is density, and Z is atomic number [10,14]. Thus, the range of a β-particle of given energy in graphite is 1.15 times its range in aluminum. To obtain the curve in Fig. 5, the approximation was made that all tritium in the graphite sample was concentrated at the mean implantation depth of 330 nm. This depth is added to the graphite thickness equivalent to the deposited aluminum, i.e., 1.15 times the thickness of the deposited layer, before using the curve in Fig. 7 to calculate the probability of emission of β particles from the surface. As the experimental measurements in Fig. 5 are only known to within a constant factor, (it is after all, a relative intensity, and not an absolute one), the theoretical curve was fitted to the data by multiplying it by a constant such that for zero deposition, it has a value of 0.65, then adding a uniform background intensity of 0.05, based on the measured relative image intensities after depositing more than 1600 nm of aluminum. The agreement between the shape of the calculated curve, and the experimentally measured points is then quite satisfactory.

5. Conclusions

Variations in tritium image intensity have been measured as a function of the depth of the tritium below the surface of the specimen being imaged, in graphite, and indirectly in aluminum. Experimentally observed trends are reasonably well modelled using a *depth dependence of image intensity* which is calculated on the basis of β transport to the surface.

It has been shown that tritium diffuses to surfaces in aluminum, and that surface conditioning in aluminum also plays a significant role in determining image intensity. It seems likely that this will apply to most metals, implying that control of the surface will be an important hurdle to overcome in developing tritium imaging as a quantitative tool. Of course, it might be conversely said that tritium imaging has the potential to examine surface conditioning in a quantitative fashion, although that concept, too, is not without its difficulties.

Acknowledgements

This work was supported by the Canadian Fusion Fuels Technology Project and the Natural Sciences and Engineering Research Council of Canada. The authors wish to thank Mr Charles Perez for his invaluable help in the construction of the apparatus used in these experiments, and Dr J.W. Davis for many insightful discussions. Thanks are also offered to Dr J.A. Sawicki, who arranged for the implantation of the specimens in the Chalk River Nuclear Laboratories' Isotope Separator, and to Dr A.B. Antoniazzi who measured the total tritium content of specimens at Ontario Hydro Kipling Laboratories. Thanks are also due to Dr Nazir Kherani, of Ontario Hydro, for making the MCSET code available to us, and to Dr W. Eckstein of IPP Garching, Germany, for use of the TRVMC Code.

References

[1] M.E. Malinowski, Appl. Phys. Lett. 39 (1981) 509.
[2] M.E. Malinowski, R.A. Causey, J. Vac. Sci. Technol. A6 (1988) 2130.
[3] K.N. Kushita, I. Youle, A.A. Haasz, J.A. Sawicki, J. Nucl. Mater. 179–181 (1991) 235.
[4] A.A. Haasz, I.S. Youle, A.B. Antoniazzi, W.T. Shmayda, J. Nucl. Mater. 220–222 (1995) 585.
[5] K.J. Hanszen, R. Lauer, in: Focusing of Charged Particles, ed. A. Septier (Academic Press, New York, 1967).
[6] J.L. Wisa, Nucl. Instrum. Methods 162 (1979) 587.
[7] W. Eckstein, C. García-Rosales, J. Roth, W. Ottenberger, Sputtering Data, IPP 9/82, Max Plank Institute für Plasmaphysik, 8046 Garching bei München, Germany, 1993.
[8] W. Eckstein, Computer Simulations of Ion-Surface Interactions, Springer Series in Materials Science, Vol. 10 (Springer, Berlin, 1991).
[9] J.A. Sawicki, J. Roth, L.M. Howe, J. Nucl. Mater. 162–164 (1989) 1019.
[10] W.T. Shmayda, Tritium Interactions with Materials (Ontario Hydro Research Division, Toronto, 1984).

[11] K. Kamada, A. Sagara, N. Sugiyama, S. Yamaguchi, J. Nucl Mater. 128&129 (1984) 664.
[12] K. Kamada, J. Nucl. Mater. 169 (1989) 141.
[13] M. von Ardenne, Tabellen zur angewandten Physik, Vol. 1 (VEB Deutscher Verlag der Wisenschaften, Berlin, 1962).
[14] N.P. Kherani, PhD thesis, University of Toronto (1993).
[15] M. Mayer, W. Eckstein, Nucl. Instrum. Methods B94 (1994) 22.
[16] J.F. Ziegler, TRIM95, IBM-Research, 28-0, Yorktown, NY 10598, USA, 1995.